1

Integration of Nonlinear Circuit Elements into FDTD Method Formulation

Joshua M. Kast and Atef Z. Elsherbeni

Colorado School of Mines, Electrical Engineering Department, Golden, CO, USA

1.1 Introduction

Over the past three decades, finite-difference time-domain (FDTD) simulations have been applied dramatically, with three key factors: innovation in simulation boundary conditions, improved capabilities of computing hardware, and novel updating equations to model special conditions within the FDTD. While FDTD simulations initially enabled the exploration of interactions between electromagnetic fields and arbitrary material geometries, a host of additional processes may now be explored by embedding lumped-circuit elements and even entire sub-circuits into FDTD simulations. With this approach, also called "lumped-element finite-difference time-domain" (LE-FDTD) or "hybrid FDTD," complex circuits may be simulated with simultaneous simulation of circuit theory and Maxwell's equations.

There are two major application areas for these evolving techniques: the design of analog microwave circuits and the design of high-speed digital circuits. In both cases, there are demands for increased frequency, bandwidth, and complexity, in addition to low energy consumption and footprint. In microwave circuits, nonlinearity is used in the design of mixers and energy-efficient amplifiers. Digital circuits, comprised of logic gates, are fundamentally nonlinear in their operation. In both cases, effects of harmonics, crosstalk, and distortion are key factors in the implementation of a design.

An important work in this area was performed by Sui et al. [1, 2], who demonstrated the extension of 2D FDTD simulations by incorporating lumped-element circuit components: resistor, capacitor, inductor, and diode, as well as a small-signal model for a transistor. This work shed light on the transmission-line method (TLM), its similarities to FDTD [3], and previous successful implementations of nonlinear components into TLM simulations [4]. In their 2D simulations,

Advances in Time-Domain Computational Electromagnetic Methods, First Edition.
Edited by Qiang Ren, Su Yan, and Atef Z. Elsherbeni.

Sui et al. demonstrated a circuit comprising a linear resistor and a nonlinear diode, which was in favorable agreement with circuit-theory SPICE-type simulations.

This work in 2D FDTD was extended by Piket-May et al. [5, 6]. In these works, several important contributions were made to the technique. First, 3D formulations were described for lumped elements including resistor, capacitor, inductor, and diode. Second, the updating formulation of diodes was modified based on [2], by replacing the explicit implementation of the Shockley diode equation by an implicit form, which was solved using Newton–Raphson iteration. Also, a bipolar junction transistor (BJT) was implemented based on the Ebers–Moll model [7], which accounts for both small- and large-signal effects. The Ebers–Moll model was implemented directly in the form of FDTD updating equations, which were solved using Newton–Raphson iteration in each FDTD time step.

An additional novel technique was presented in [5]: a software link between an FDTD simulator and a circuit-theory SPICE simulator [8]. The possibility of integrating a time-domain circuit simulator into the FDTD is extremely appealing because it enables the integration of lumped elements, or even sub-circuits into an FDTD simulation, without the need to create bespoke updating equations for each sub-circuit. A wealth of semiconductor formulations within SPICE [9] may be readily incorporated into the FDTD. While the FDTD–SPICE connection was successfully demonstrated, accuracy and stability problems were encountered with microstrip geometries commonly used for microwave circuits [5]. Nonetheless, this work laid important foundations for future developments in the field.

Based on these foundational works, numerous approaches have been described for simulating FDTD with integrated lumped elements, sub-circuits, and active semiconductor devices. We broadly divide these into three categories for further discussion. The first category is specialized updating equations used to simulate a specific type of component within the FDTD. The second category is co-simulation approaches, such as the one described in [5], where an offboard circuit simulator is used to model the activity of a sub-circuit or circuit element. The third category includes data-based models, which emulate the behavior of a device based on stored measurement or simulation data (often *S*-parameters).

1.2 FDTD Updating Equations for Nonlinear Elements

Initial efforts to incorporate lumped-element devices into the FDTD focused primarily on developing specialized updating formulations for Yee cells occupied by circuit components [2, 6]. This is an advantageous approach because circuit components may be updated using the same central difference (second-order accurate) differentiation scheme used for updating the electric and magnetic fields. Also, the

computational overhead is minimized when separate simulation engines are not invoked.

As a basis for further discussion, we assume an FDTD simulation with an electric-field updating equation of the form:

$$\begin{aligned} E_z\big|_{i,j,k}^{n+1} = {} & \frac{2\varepsilon_z\big|_{i,j,k} - \Delta t\,\sigma_z^e\big|_{i,j,k}}{2\varepsilon_z\big|_{i,j,k} + \Delta t\,\sigma_z^e\big|_{i,j,k}} E_z\big|_{i,j,k}^{n} \\ & + \frac{2\Delta t}{\left(2\varepsilon_z\big|_{i,j,k} + \Delta t\,\sigma_z^e\big|_{i,j,k}\right)\Delta x}\left(H_y\big|_{i,j,k}^{n+\frac{1}{2}} - H_y\big|_{i-1,j,k}^{n+\frac{1}{2}}\right) \\ & - \frac{2\Delta t}{\left(2\varepsilon_z\big|_{i,j,k} + \Delta t\,\sigma_z^e\big|_{i,j,k}\right)\Delta y}\left(H_x\big|_{i,j,k}^{n+\frac{1}{2}} - H_x\big|_{i,j-1,k}^{n+\frac{1}{2}}\right) \\ & - \frac{2\Delta t}{2\varepsilon_z\big|_{i,j,k} + \Delta t\,\sigma_z^e\big|_{i,j,k}} J_{iz}\big|_{i,j,k}^{n+\frac{1}{2}} \end{aligned} \tag{1.1}$$

and with magnetic fields updated by:

$$\begin{aligned} H_z\big|_{i,j,k}^{n+\frac{1}{2}} = {} & \frac{2\mu_z\big|_{i,j,k} - \Delta t\,\sigma_z^m\big|_{i,j,k}}{2\mu_z\big|_{i,j,k} + \Delta t\,\sigma_z^m\big|_{i,j,k}} H_z\big|_{i,j,k}^{n-\frac{1}{2}} \\ & + \frac{2\Delta t}{\left(2\mu_z\big|_{i,j,k} + \Delta t\,\sigma_z^m\big|_{i,j,k}\right)\Delta y}\left(E_x\big|_{i,j+1,k}^{n} - E_x\big|_{i,j,k}^{n}\right) \\ & - \frac{2\Delta t}{\left(2\mu_z\big|_{i,j,k} + \Delta t\,\sigma_z^m\big|_{i,j,k}\right)\Delta x}\left(E_y\big|_{i+1,j,k}^{n} - E_y\big|_{i,j,k}^{n}\right) \\ & - \frac{2\Delta t}{2\mu_z\big|_{i,j,k} + \Delta t\,\sigma_z^m\big|_{i,j,k}} M_{iz}\big|_{i,j,k}^{n} \end{aligned} \tag{1.2}$$

These equations are similar to those listed in [6] and are based on the notation and parameter definitions in [10].

1.2.1 Junction Diode

The diode serves as an excellent model for the integration of a nonlinear device into FDTD: it is passive, has only two ports, and can occupy one FDTD cell. The diode was integrated into 2D FDTD by Sui et al. [2], and this approach was improved and extended to 3D FDTD by Piket-May et al. [6]. Both methods use the "ideal" diode equation proposed by Shockley [11]:

$$I_D = I_S\left(e^{\frac{qV_D}{\eta kT}} - 1\right) \tag{1.3}$$

In this equation, the current through the diode I_D is a function of the voltage across the diode V_D, as well as several physical properties of the

diode: temperature T and the ideality factor η. These are related by q and K: the charge of an electron and Boltzmann's constant, respectively.

We may adapt (1.1) for a diode pointing in the negative z direction by incorporating (1.3) and understanding that the voltage across the diode V_D at time step $n+\frac{1}{2}$ will be $V_D\big|^{n+\frac{1}{2}} = \Delta z \frac{E_z\big|^{n}_{i,j,k} + E_z\big|^{n+1}_{i,j,k}}{2}$. The current density through the cell $J_{iz}\big|_{i,j,k}$ is replaced by the diode current and the cross-sectional area of the cell $\left(\frac{I_D}{\Delta x \Delta y}\right)$, giving:

$$
\begin{aligned}
E_z\big|^{n+1}_{i,j,k} = {} & \frac{2\varepsilon_z\big|_{i,j,k} - \Delta t\, \sigma^e_z\big|_{i,j,k}}{2\varepsilon_z\big|_{i,j,k} + \Delta t\, \sigma^e_z\big|_{i,j,k}}\, E_z\big|^{n}_{i,j,k} \\
& + \frac{2\Delta t}{\left(2\varepsilon_z\big|_{i,j,k} + \Delta t\, \sigma^e_z\big|_{i,j,k}\right)\Delta x}\left(H_y\Big|^{n+\frac{1}{2}}_{i,j,k} - H_y\Big|^{n+\frac{1}{2}}_{i-1,j,k}\right) \\
& - \frac{2\Delta t}{\left(2\varepsilon_z\big|_{i,j,k} + \Delta t\, \sigma^e_z\big|_{i,j,k}\right)\Delta y}\left(H_x\Big|^{n+\frac{1}{2}}_{i,j,k} - H_x\Big|^{n+\frac{1}{2}}_{i,j-1,k}\right) \\
& - \frac{2\Delta t}{2\varepsilon_z\big|_{i,j,k} + \Delta t\, \sigma^e_z\big|_{i,j,k}} \frac{I_S\left(e^{\frac{q\Delta z\left(E_z\big|^{n}_{i,j,k} + E_z\big|^{n+1}_{i,j,k}\right)}{2\eta kT}} - 1\right)}{\Delta x \Delta y}
\end{aligned}
\tag{1.4}
$$

The transcendental Eq. (1.4) cannot be solved analytically. In the work of Sui et al. this problem was resolved by calculating V_D based only on the value of $E_z\big|^{n}_{i,j,k}$ [2], which limited the approach to only very small time steps and low voltages across the diode. A more capable approach, proposed by Piket-May, uses an iterative process to resolve (1.4). In this method, we rearrange (1.4) as follows:

$$
\begin{aligned}
f\left(E_z\big|^{n}_{i,j,k}\right) = {} & \frac{2\Delta t}{2\varepsilon_z\big|_{i,j,k} + \Delta t\, \sigma^e_z\big|_{i,j,k}} \frac{I_S}{\Delta x \Delta y} e^{\frac{q\,\Delta z E_z\big|^{n}_{i,j,k}}{2\eta kT}} e^{\frac{q\,E_z\big|^{n+1}_{i,j,k}}{2\eta kT}} + E_z\big|^{n+1}_{i,j,k} \\
& - \frac{2\Delta t}{2\varepsilon_z\big|_{i,j,k} + \Delta t\, \sigma^e_z\big|_{i,j,k}} \frac{I_S}{\Delta x \Delta y} - \frac{2\varepsilon_z\big|_{i,j,k} - \Delta t\, \sigma^e_z\big|_{i,j,k}}{2\varepsilon_z\big|_{i,j,k} + \Delta t\, \sigma^e_z\big|_{i,j,k}}\, E_z\big|^{n}_{i,j,k} \\
& - \frac{2\Delta t}{\left(2\varepsilon_z\big|_{i,j,k} + \Delta t\, \sigma^e_z\big|_{i,j,k}\right)\Delta x}\left(H_y\Big|^{n+\frac{1}{2}}_{i,j,k} - H_y\Big|^{n+\frac{1}{2}}_{i-1,j,k}\right) \\
& + \frac{2\Delta t}{\left(2\varepsilon_z\big|_{i,j,k} + \Delta t\, \sigma^e_z\big|_{i,j,k}\right)\Delta y}\left(H_x\Big|^{n+\frac{1}{2}}_{i,j,k} - H_x\Big|^{n+\frac{1}{2}}_{i,j-1,k}\right)
\end{aligned}
\tag{1.5}
$$

with the goal of creating an equation with the format of $f(x) = Ae^{Bx} + x + C$ and finding the root where $f(x) = 0$. In this case:

$$
\begin{aligned}
A &= \frac{2\Delta t}{2\varepsilon_z\big|_{i,j,k} + \Delta t\,\sigma_z^e\big|_{i,j,k}} \frac{I_S}{\Delta x \Delta y} e^{\frac{q\Delta z\, E_z\big|_{i,j,k}^n}{2\eta kT}} \\
B &= \frac{q\Delta z}{2\eta kT} \\
C &= -\frac{2\Delta t}{2\varepsilon_z\big|_{i,j,k} + \Delta t\,\sigma_z^e\big|_{i,j,k}} \frac{I_S}{\Delta x \Delta y} - \frac{2\varepsilon_z\big|_{i,j,k} - \Delta t\,\sigma_z^e\big|_{i,j,k}}{2\varepsilon_z\big|_{i,j,k} + \Delta t\,\sigma_z^e\big|_{i,j,k}} E_z\big|_{i,j,k}^n \\
&\quad - \frac{2\Delta t}{\left(2\varepsilon_z\big|_{i,j,k} + \Delta t\,\sigma_z^e\big|_{i,j,k}\right)\Delta x} \left(H_y\big|_{i,j,k}^{n+\frac{1}{2}} - H_y\big|_{i-1,j,k}^{n+\frac{1}{2}} \right) \\
&\quad + \frac{2\Delta t}{\left(2\varepsilon_z\big|_{i,j,k} + \Delta t\,\sigma_z^e\big|_{i,j,k}\right)\Delta y} \left(H_x\big|_{i,j,k}^{n+\frac{1}{2}} - H_x\big|_{i,j-1,k}^{n+\frac{1}{2}} \right)
\end{aligned}
\tag{1.6}
$$

Given an initial guess for the quantity x, we may improve upon it by solving the following one:

$$
x_{\text{updated}} = x - \frac{f(x)}{f'(x)} = x - \frac{Ae^{Bx} + x + C}{ABe^{Bx} + 1} \tag{1.7}
$$

By iteratively solving (1.7), with the constants found in (1.6), the updated value of the electric field across the diode $E_z\big|_{i,j,k}^{n+1}$ may be calculated, while preserving the second-order accuracy and central difference nature of the FDTD formulation.

A further improvement of this technique was proposed by Ciampolini et al. [12], who provided a more sophisticated model of the junction diode, which includes its nonlinear capacitance, as illustrated in Figure 1.1. In their model, the total

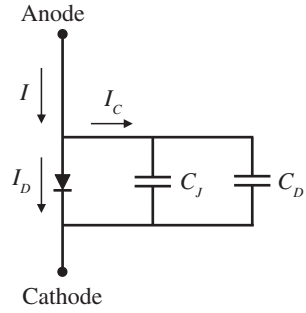

Figure 1.1 Improved model of junction diode incorporating junction and diffusion capacitance.

capacitance of a diode C_D is the sum of the junction capacitance C_J and the diffusion capacitance C_D. Both capacitance values are functions of the current through the diode I_D.

The total current through the diode I is given by:

$$I|^{n+\frac{1}{2}} = I_D|^{n+\frac{1}{2}} + \left[C_J|^{n+\frac{1}{2}} + C_D|^{n+\frac{1}{2}} \right] \frac{V_D|^{n+1} - V_D|^{n}}{\Delta t} \tag{1.8}$$

In this equation, capacitance values are time dependent because they depend on the voltage across the diode V_D. The diffusion capacitance is calculated as:

$$C_D(V_D) = \frac{q}{KT} \tau_D I_S \left(e^{\frac{qV_D}{KT}} - 1 \right) \tag{1.9}$$

where τ_D is the diode's transit time. The junction capacitance is a piecewise function of V_D:

$$C_J(V_D) = \begin{cases} C_{J0} \left(1 - \frac{V_D}{\Phi_0} \right)^{-m} & \text{if } V_D < F_C \cdot \Phi_0 \\ \frac{C_{J0}}{(1 - F_C)^{1+m}} \left((1 - F_C(1+m)) - \frac{m \cdot V_D}{\Phi_0} \right) & \text{if } V_D \geq F_C \cdot \Phi_0 \end{cases} \tag{1.10}$$

The values m and F_C are specific to each model of diode and relate to its composition. The value Φ_0 is the "built-in voltage" of the diode, with a default value in SPICE2 of 1 V (but this value may change depending on the specific diode used) [9].

This addition of nonlinear capacitance allows for a more nuanced model of the diode to be incorporated into an FDTD simulation. Ciampolini et al. noted that it is still possible to use Newton–Raphson iteration to resolve self-referential updating equations. However, the increased complexity of the equations and the piecewise nature of (1.10) impose additional demands on the numerical method. To maintain stability in the updating solutions, very short time steps (below the Courant-Friedrichs-Lewy [CFL] limit) and a "damped" Newton–Raphson method were required [12].

1.2.2 Bipolar Junction Transistors: Small-Signal Model

To simulate active devices such as amplifiers, it is often necessary to incorporate a transistor model into a circuit or full-wave simulation. BJTs are commonly employed in analog and radio frequency (RF) electronic devices, and they are capable of both linear and nonlinear modes of operation. During linear operation in the forward-active mode, a BJT may be modeled as a current-controlled current source, as described in [13] and shown in Figure 1.2. The values of the parameters α, R_e, and R_o depend on the type of the transistor, and the selected direct current (DC) operating point, as determined by supply voltage and bias resistors.

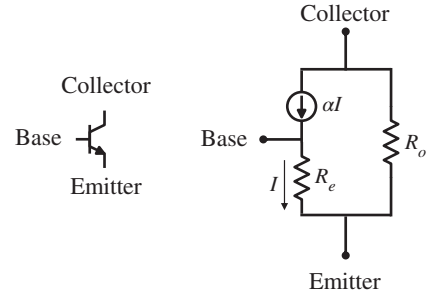

Figure 1.2 Schematic symbol and small-signal model of bipolar junction transistor.

ElMahgoub and Elsherbeni described the introduction of multiple types of dependent sources into FDTD [14], including voltage-controlled voltage sources, voltage-controlled current sources, current-controlled voltage sources, and current-controlled current sources. This selection of dependent sources enables the implementation of small-signal amplifier and transistor models in FDTD.

In [14], the BJT was simulated by first designing a BJT common-collector amplifier circuit and then determining the amplifier's DC operating condition. Next, the updating Eq. (1.1) was modified to function as a current-controlled current source:

$$\begin{aligned} E_z\big|_{i,j,k}^{n+1} = {} & \frac{2\varepsilon_z\big|_{i,j,k} - \Delta t\,\sigma_z^e\big|_{i,j,k}}{2\varepsilon_z\big|_{i,j,k} + \Delta t\,\sigma_z^e\big|_{i,j,k}} E_z\big|_{i,j,k}^{n} \\ & + \frac{2\Delta t}{\left(2\varepsilon_z\big|_{i,j,k} + \Delta t\,\sigma_z^e\big|_{i,j,k}\right)\Delta x}\left(H_y\big|_{i,j,k}^{n+\frac{1}{2}} - H_y\big|_{i-1,j,k}^{n+\frac{1}{2}}\right) \\ & - \frac{2\Delta t}{\left(2\varepsilon_z\big|_{i,j,k} + \Delta t\,\sigma_z^e\big|_{i,j,k}\right)\Delta y}\left(H_x\big|_{i,j,k}^{n+\frac{1}{2}} - H_x\big|_{i,j-1,k}^{n+\frac{1}{2}}\right) \\ & + \frac{2\Delta t}{\Delta x\Delta y\left(2\varepsilon_z\big|_{i,j,k} + \Delta t\,\sigma_z^e\big|_{i,j,k}\right)}\alpha I_{z\,\text{sampled}}\Big|_{i,j,k}^{n+\frac{1}{2}} \end{aligned} \tag{1.11}$$

In this modified updating equation, the variable $I_{z\,\text{sampled}}\Big|_{i,j,k}^{n+\frac{1}{2}}$ is the current at another location in the circuit, sampled by integration of the magnetic field following Ampere's law. The constant α is the gain of the dependent source and is chosen depending on the DC analysis of the transistor [13].

In the work of [14], the active component of the transistor was simulated by the current-controlled current source updating equation of (1.11). The bias resistors were modeled using lumped-element FDTD components, following the formulations of [14]. When the amplifier circuit was excited by a sinusoidal waveform, the circuit was seen to function as a voltage amplifier with a high gain. The output voltage observed in the FDTD simulation was comparable favorably with analytical predictions, demonstrating the feasibility of this small-signal approach.

1.2.3 Bipolar Junction Transistors: Ebers–Moll Model

The formulation for simulation of a nonlinear BJT may be viewed as an extension of the formulation for the junction diode. The BJT is a three-terminal device wherein the flow of current from the collector terminal to the emitter is controlled by the current applied at the base. In the Ebers–Moll model [7], the two PN semiconductor junctions of the BJT are modeled as junction diodes and the current flow is modeled using dependent current sources, as shown in Figure 1.3.

Following the formulation of [5], we will develop an FDTD updating formulation for the BJT. This three-terminal device spans two cells, with two distinct voltages, the base–collector voltage V_{BC} and the base–emitter voltage V_{BE}. These voltages are related to the electric fields within the Yee cells at time step $n+\frac{1}{2}$ by:

$$V_{BC}\Big|^{n+\frac{1}{2}} = \Delta z \frac{E_z\big|_{BC}^{n} + E_z\big|_{BC}^{n+1}}{2} \tag{1.12}$$

and

$$V_{BE}\Big|^{n+\frac{1}{2}} = -\Delta z \frac{E_z\big|_{EB}^{n} + E_z\big|_{EB}^{n+1}}{2} \tag{1.13}$$

We adapt (1.4) to solve for $E_z\big|_{BC}^{n+1}$. We assume that $\sigma_z^e = 0$ within this region:

$$\begin{aligned} E_z\big|_{BC}^{n+1} = E_z\big|_{BC}^{n} &+ \frac{\Delta t}{\varepsilon_z\big|_{BC}\Delta x}\left(H_y\Big|_{BC}^{n+\frac{1}{2}} - H_y\Big|_{BC+(-1,0,0)}^{n+\frac{1}{2}}\right) \\ &- \frac{\Delta t}{\varepsilon_z\big|_{BC}\Delta y}\left(H_x\Big|_{BC}^{n+\frac{1}{2}} - H_x\Big|_{BC+(0,-1,0)}^{n+\frac{1}{2}}\right) \\ &- \frac{\Delta t}{\varepsilon_z\big|_{BC}} \frac{I_S\left(e^{\frac{q\Delta z\left(E_z\big|_{BC}^{n} + E_z\big|_{BC}^{n+1}\right)}{2\eta kT}} - 1\right) - \alpha_F I_S\left(e^{\frac{-q\Delta z\left(E_z\big|_{EB}^{n} + E_z\big|_{EB}^{n+1}\right)}{2\eta kT}} - 1\right)}{\Delta x \Delta y} \end{aligned} \tag{1.14}$$

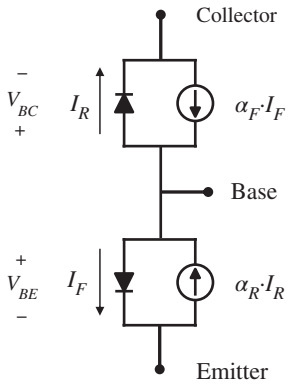

Figure 1.3 Ebers–Moll model of a bipolar junction transistor.

For $E_z|_{EB}^{n+1}$, we find a similar expression:

$$E_z|_{EB}^{n+1} = E_z|_{EB}^{n} + \frac{\Delta t}{\varepsilon_z|_{EB}\Delta x}\left(H_y\Big|_{EB}^{n+\frac{1}{2}} - H_y\Big|_{EB+(-1,0,0)}^{n+\frac{1}{2}}\right) - \frac{\Delta t}{\varepsilon_z|_{EB}\Delta y}\left(H_x\Big|_{EB}^{n+\frac{1}{2}} - H_x\Big|_{EB+(0,-1,0)}^{n+\frac{1}{2}}\right) - \frac{\Delta t}{\varepsilon_z|_{EB}}\frac{\alpha_R I_S\left(e^{\frac{q\Delta z\left(E_z|_{BC}^{n}+E_z|_{BC}^{n+1}\right)}{2\eta kT}}-1\right) - I_S\left(e^{\frac{-q\Delta z\left(E_z|_{EB}^{n}+E_z|_{EB}^{n+1}\right)}{2\eta kT}}-1\right)}{\Delta x\Delta y} \tag{1.15}$$

These expressions are rearranged to form a pair of expressions in the following format:

$$f_1(\vec{x}) = \boldsymbol{A}_{1,1}e^{B_{1,1}\vec{x}_1} + \boldsymbol{A}_{1,2}e^{\boldsymbol{B}_{1,2}\vec{x}_2} + \vec{x}_1 + \vec{C}_1$$
$$f_2(\vec{x}) = \boldsymbol{A}_{2,1}e^{B_{2,1}\vec{x}_1} + \boldsymbol{A}_{2,2}e^{\boldsymbol{B}_{2,2}\vec{x}_2} + \vec{x}_2 + \vec{C}_2 \tag{1.16}$$

as:

$$\begin{aligned} f_1\left(\left[E_z|_{EB}^{n+1}, E_z|_{BC}^{n+1}\right]^T\right) = {} & \frac{\Delta t I_S e^{\frac{q\Delta z\,E_z|_{BC}^{n}}{2\eta kT}}}{\varepsilon_z|_{BC}\Delta x\Delta y}e^{\frac{q\,\Delta z E_z|_{BC}^{n+1}}{2\eta kT}} \\ & - \frac{\Delta t\alpha_F I_S e^{\frac{-q\,\Delta z E_z|_{EB}^{n}}{2\eta kT}}}{\varepsilon_z|_{BC}\Delta x\Delta y}e^{\frac{-q\Delta z\,E_z|_{EB}^{n+1}}{2\eta kT}} + E_z|_{BC}^{n+1} \\ & - E_z|_{BC}^{n} - \frac{\Delta t}{\varepsilon_z|_{BC}\Delta x}\left(H_y\Big|_{BC}^{n+\frac{1}{2}} - H_y\Big|_{BC+(-1,0,0)}^{n+\frac{1}{2}}\right) \\ & + \frac{\Delta t}{\varepsilon_z|_{BC}\Delta y}\left(H_x\Big|_{BC}^{n+\frac{1}{2}} - H_x\Big|_{BC+(0,-1,0)}^{n+\frac{1}{2}}\right) \\ & + (\alpha_F - 1)\frac{\Delta t I_S}{\varepsilon_z|_{BC}\Delta x\Delta y} \end{aligned} \tag{1.17}$$

and

$$\begin{aligned} f_2\left(\left[E_z|_{EB}^{n+1}, E_z|_{BC}^{n+1}\right]^T\right) = {} & \frac{\Delta t\alpha_R I_S e^{\frac{q\Delta z\,E_z|_{BC}^{n}}{2\eta kT}}}{\varepsilon_z|_{EB}\Delta x\Delta y}e^{\frac{q\,\Delta z E_z|_{BC}^{n+1}}{2\eta kT}} \\ & - \frac{\Delta t I_S e^{\frac{-q\Delta z\,E_z|_{EB}^{n}}{2\eta kT}}}{\varepsilon_z|_{EB}\Delta x\Delta y}e^{\frac{-q\,\Delta z E_z|_{EB}^{n+1}}{2\eta kT}} + E_z|_{EB}^{n+1} \\ & - E_z|_{EB}^{n} - \frac{\Delta t}{\varepsilon_z|_{EB}\Delta x}\left(H_y\Big|_{EB}^{n+\frac{1}{2}} - H_y\Big|_{EB+(-1,0,0)}^{n+\frac{1}{2}}\right) \\ & + \frac{\Delta t}{\varepsilon_z|_{EB}\Delta y}\left(H_x\Big|_{EB}^{n+\frac{1}{2}} - H_x\Big|_{EB+(0,-1,0)}^{n+\frac{1}{2}}\right) \\ & + (1 - \alpha_R)\frac{\Delta t I_S}{\varepsilon_z|_{EB}\Delta x\Delta y} \end{aligned} \tag{1.18}$$

The values of $E_z|_{EB}^{n+1}$ and $E_z|_{BC}^{n+1}$ are numerically approximated by iterating:

$$\vec{x}^{\text{updated}} = \vec{x} - \boldsymbol{F}^{-1}(\vec{x}) f(\vec{x}) \tag{1.19}$$

where

$$\boldsymbol{F}(\vec{x}) = \begin{bmatrix} \dfrac{\partial f_1(\vec{x})}{\partial \vec{x}_1} & \dfrac{\partial f_1(\vec{x})}{\partial \vec{x}_2} \\ \dfrac{\partial f_2(\vec{x})}{\partial \vec{x}_1} & \dfrac{\partial f_2(\vec{x})}{\partial \vec{x}_2} \end{bmatrix} \tag{1.20}$$

Iteration of (1.19) is carried out until the solution converges satisfactorily, by ensuring that $|\vec{x}^{\text{updated}} - \vec{x}|$ reaches a sufficiently low value. When this technique is applied in circuits with realistic biasing configurations (source voltages and resistances), functional amplifiers may be modeled with the transistor capable of operating in the cut-off, active, and saturation modes [5].

The work of Ciampolini et al. on an improved diode model suggests similar possibilities for the simulation of BJTs [12]. Indeed, in a follow-up work on this subject, the authors demonstrated the extension of the Ebers–Moll model by simulating a BJT having nonlinear capacitances on its emitter–base and base–collector junctions [15]. This is achieved quite simply as extensions of (1.14) and (1.15), which incorporate the nonlinear capacitances of (1.9) and (1.10). We write these modified updating expressions as follows:

$$\begin{aligned} E_z|_{BC}^{n+1} = {} & E_z|_{BC}^{n} + \frac{\Delta t}{\varepsilon_z|_{BC}\Delta x}\left(H_y\Big|_{BC}^{n+\frac{1}{2}} - H_y\Big|_{BC+(-1,0,0)}^{n+\frac{1}{2}}\right) \\ & - \frac{\Delta t}{\varepsilon_z|_{BC}\Delta y}\left(H_x\Big|_{BC}^{n+\frac{1}{2}} - H_x\Big|_{BC+(0,-1,0)}^{n+\frac{1}{2}}\right) - \frac{\Delta t}{\varepsilon_z|_{BC}\Delta x\Delta y} \\ & \times \left(\begin{array}{l} I_S\left(e^{\frac{q\Delta z\left(E_z|_{BC}^{n} + E_z|_{BC}^{n+1}\right)}{2\eta kT}} - 1\right) - \alpha_F I_S\left(e^{\frac{-q\Delta z\left(E_z|_{EB}^{n} + E_z|_{EB}^{n+1}\right)}{2\eta kT}} - 1\right) \\ \quad + \left(C_{JBC}\left(-\Delta z\dfrac{E_z|_{BC}^{n} + E_z|_{BC}^{n+1}}{2}\right)\right. \\ \quad \left. + C_{DBC}\left(-\Delta z\dfrac{E_z|_{BC}^{n} + E_z|_{BC}^{n+1}}{2}\right)\right)\Delta z\dfrac{E_z|_{BC}^{n+1} - E_z|_{BC}^{n}}{\Delta t} \end{array} \right) \end{aligned} \tag{1.21}$$

and

$$\begin{aligned} E_z|_{EB}^{n+1} = {} & E_z|_{EB}^{n} + \frac{\Delta t}{\varepsilon_z|_{EB}\Delta x}\left(H_y\Big|_{EB}^{n+\frac{1}{2}} - H_y\Big|_{EB+(-1,0,0)}^{n+\frac{1}{2}}\right) \\ & - \frac{\Delta t}{\varepsilon_z|_{EB}\Delta y}\left(H_x\Big|_{EB}^{n+\frac{1}{2}} - H_x\Big|_{EB+(0,-1,0)}^{n+\frac{1}{2}}\right) - \frac{\Delta t}{\varepsilon_z|_{EB}\Delta x\Delta y} \end{aligned}$$

$$\times \left(\begin{array}{l} \alpha_R I_S \left(e^{\frac{q\Delta z\left(E_z|_{BC}^{n} + E_z|_{BC}^{n+1} \right)}{2\eta kT}} - 1 \right) - I_S \left(e^{\frac{-q\Delta z\left(E_z|_{EB}^{n} + E_z|_{EB}^{n+1} \right)}{2\eta kT}} - 1 \right) \\ \quad + \left(C_{JEB} \left(\Delta z \dfrac{E_z|_{EB}^{n} + E_z|_{EB}^{n+1}}{2} \right) \right. \\ \quad \left. + C_{DEB} \left(\Delta z \dfrac{E_z|_{EB}^{n} + E_z|_{EB}^{n+1}}{2} \right) \right) \Delta z \dfrac{E_z|_{EB}^{n+1} - E_z|_{EB}^{n}}{\Delta t} \end{array} \right) \tag{1.22}$$

As noted in [12], the additional complexity of these updating equations, with their multiple (and piecewise) nonlinear elements, imposes increased demands on the numerical computations required for these updating equations. In [15], a time-adaptive technique has been proposed, where failure of Newton–Raphson iteration to converge signals a reduction in Δt of the FDTD simulation. This feature is of particular necessity for signals with abrupt transitions.

1.2.4 Bipolar Junction Transistors: Gummel–Poon Model

Improvements upon the Ebers–Moll BJT model were proposed by Gummel and Poon [16]. This model for the BJT is widely used in simulation programs including SPICE, and when certain device constants are omitted, it becomes equivalent to the Ebers–Moll model [9]. The schematic representation of the Gummel–Poon model is shown in Figure 1.4.

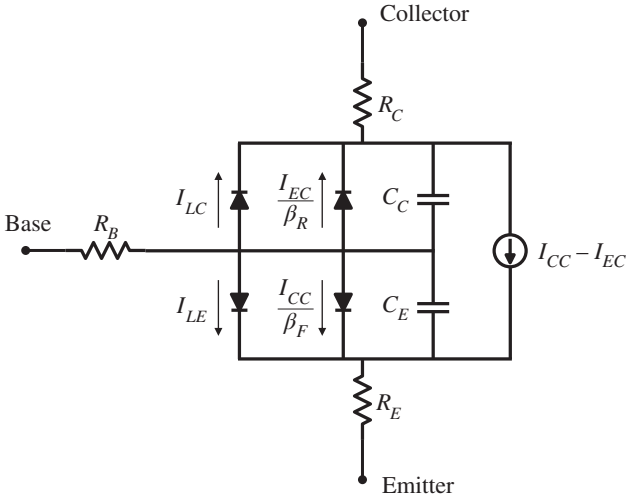

Figure 1.4 Gummel–Poon model of a bipolar junction transistor.

We write a subset of this model, with the current at the collector after [17] as follows:

$$I_C = I_{LC} + \left(1 + \frac{1}{\beta_R}\right) I_{EC} - I_{CC} + C_C \frac{\partial V_{BC}}{\partial t} \tag{1.23}$$

and at the emitter:

$$I_E = -\left(I_{LE} + \left(1 + \frac{1}{\beta_F}\right) I_{CC} - I_{EC} + C_E \frac{\partial V_{BE}}{\partial t}\right) \tag{1.24}$$

where

$$I_{CC} = \frac{I_S}{q_b}\left(e^{\frac{qV_{BE}}{n_F kT}} - 1\right)$$

$$I_{LE} = I_{SE}\left(e^{\frac{qV_{BE}}{n_E kT}} - 1\right)$$

$$I_{EC} = \frac{I_S}{q_b}\left(e^{\frac{qV_{BC}}{n_R kT}} - 1\right)$$

and

$$I_{LC} = I_{SC}\left(e^{\frac{qV_{BC}}{n_C kT}} - 1\right)$$

where q_b is given by:

$$q_b = \frac{1}{2} + \frac{V_{BE}}{2V_B} + \frac{V_{BC}}{2V_A} + \sqrt{\left(\frac{1}{2} + \frac{V_{BE}}{2V_B} + \frac{V_{BC}}{2V_A}\right)^2 + \frac{I_{SS}}{I_{KF}}\left(e^{\frac{qV_{BE}}{n_F kT}} - 1\right) + \frac{I_{SS}}{I_{KR}}\left(e^{\frac{qV_{BC}}{n_R kT}} - 1\right)} \tag{1.25}$$

Nonlinear capacitances, resulting from junction and diffusion effects, can be found by the piecewise expressions:

$$C_E = \begin{cases} \tau_F \dfrac{\partial I_{CC}}{\partial V_{BE}} + C_{JE}\left(1 - \dfrac{V_{BE}}{\Phi_E}\right)^{-m_E} & \text{if } V_{BE} < (FC \cdot \Phi_E) \\ \tau_F \dfrac{\partial I_{CC}}{\partial V_{BE}} + \dfrac{C_{JE}}{F_{2E}}\left(F_{3E} - \dfrac{m_E V_{BE}}{\Phi_E}\right) & \text{if } V_{BE} \geq (FC \cdot \Phi_E) \end{cases} \tag{1.26}$$

and

$$C_C = \begin{cases} \tau_R \dfrac{\partial I_{EC}}{\partial V_{BC}} + C_{JC}\left(1 - \dfrac{V_{BC}}{\Phi_C}\right)^{-m_C} & \text{if } V_{BC} < (FC \cdot \Phi_C) \\ \tau_R \dfrac{\partial I_{EC}}{\partial V_{BC}} + \dfrac{C_{JC}}{F_{2C}}\left(F_{3C} - \dfrac{m_C V_{BC}}{\Phi_C}\right) & \text{if } V_{BC} \geq (FC \cdot \Phi_C) \end{cases} \tag{1.27}$$

The terms F_{2E} and F_{2C} are calculated as follows:

$$F_{2\_} = (1 - FC)^{1+m\_}$$

and F_{3C} and F_{3C}:

$$F_{3\_} = 1 - FC \cdot (1 + m\_)$$

Definitions for constant terms are listed in Table 1.1 after [9, 17]. Where applicable, default values used in the SPICE2 program are listed. Note that when these default values are applied, the additional effects of the Gummel–Poon model are negated, and the model reduces to the Ebers–Moll formulation.

Implementation of the Gummel–Poon model for FDTD simulation poses many of the challenges similar to that of the modified Ebers–Moll model in [15]. Namely, the updating equations become significantly more complex, and the nonlinear equations defining the capacitance can exceed the capabilities of the Newton–Raphson method for small time step values near the CFL limit. This challenge is particularly acute for the simulation of the BJT, where a two-dimensional implementation of Newton–Raphson iteration is required.

Table 1.1 Description of numerical constants for the Gummel–Poon BJT model.

Symbol	Description	Default value	Unit
β_F, β_R	Ideal maximum beta (forward, reverse)	100, 1	
n_F, n_R	Current emission coefficient (forward, reverse)	1	
n_C	Base–collector leakage current emission coefficient	2	
V_A, V_B	Early voltage (forward, reverse)	∞	V
I_S	Saturation current	10^{-16}	A
I_{SE}, I_{SC}	Leakage saturation current (base–emitter, base–collector)	0	A
I_{KF}, I_{KR}	Corner for β high-current roll-off (forward, reverse)	∞	A
τ_F, τ_R	Ideal transit time (forward, reverse)	0	s
C_{JE}, C_{JC}	Zero-bias capacitance (base–emitter, base–collector)	0	F
Φ_E, Φ_C	Junction built-in potential (base–emitter, base–collector)	0.75	V
m_E, m_C	Junction grading coefficient	0.33	
FC	Forward bias depletion capacitance coefficient	0.5	

One example of a BJT simulated using FDTD is reported by Kung and Chuah [17]. In their work, the process for updating the emitter and collector current at time step $n + \frac{1}{2}$ begins by creating Taylor expansions for (1.23) and (1.24) at time n. In this approach, the need for numerical approximation of nonlinear equations is avoided, and reasonable accuracy can be achieved when sufficient terms are used to describe the Taylor series. Good accuracy and stability are provided by this approach, but the authors note that harmonics produced by nonlinear devices may exceed the capability of absorbing boundaries, leading to high-frequency modes accumulating in the simulation.

The current state of the art in BJT simulation using FDTD appears to remain a Taylor approximation of the Gummel–Poon model. This is likely due to the great complexity of FDTD updating equations based on the full Gummel–Poon formulation and small benefits provided beyond the Taylor approximation. An extension of the work in [17] includes the estimation of thermal self-heating effects during each simulation step, but retains the Taylor approximation for the transistor model.

1.2.5 Field-Effect Transistors: Small-Signal Modeling

Field-effect transistors are commonly employed in RF circuits, owing to higher frequencies of operation, lower noise figure, and capability for high-power operation [18]. Because small-signal models only address the transistor's linear region of operation, they apply primarily to the design of class A amplifiers [19]. Nonetheless, the small-signal approach forms the basis for introductions to amplifier design, including those of [20, 21], as it effectively addresses input matching, output matching, and stability issues under linear operation.

Lumped-circuit models may be embedded into FDTD simulations by using the approach described in [22]: at each time step, current at a port within the FDTD simulation is updated as a function of voltage, where the capacitance of the FDTD cell is accounted for in the updating formulation. For complex circuit models, an external simulation program such as SPICE may be used to update the state equations of the circuit model during each time step, with resulting current values passed back to the FDTD simulation during the electric-field-updating step.

A widely used 15-element field-effect transistor (FET) model [23] is illustrated in Figure 1.5. In this type of model, the active effect of the transistor is emulated by means of a controlled current source. Non-ideality of the transistor is emulated by capacitors, resistors, and inductors. Additionally, the effect of the transistor packaging is modeled by two capacitors C_{pd} and C_{pg}. In more advanced formulations, additional components are introduced to increase the accuracy of the model, and resistance or capacitance values are varied nonlinearly as a function of the current through the model.

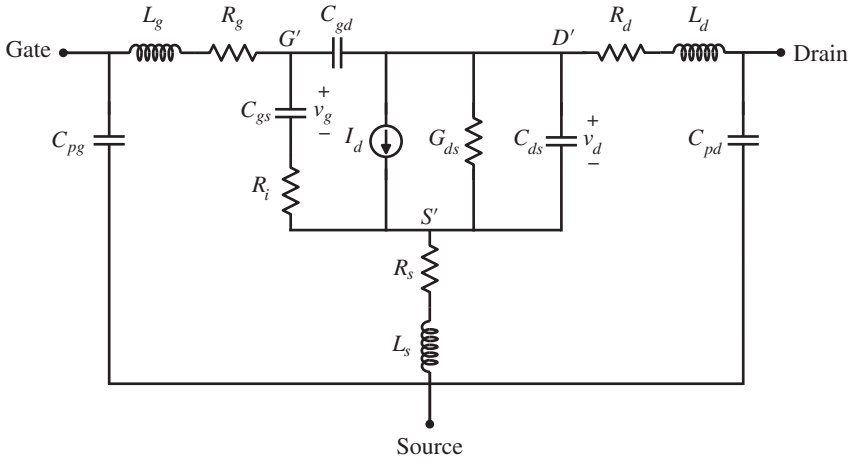

Figure 1.5 Field-effect transistor model.

Kuo et al. introduced a model similar to that in Figure 1.5 into an FDTD simulation at the junction of two transmission lines, with provisions for DC-bias current to be applied [24, 25]. The circuit was simulated in FDTD using two separate approaches: an FDTD–SPICE linked simulation as described in [22] and a direct incorporation of a circuit state-space model into the FDTD updating formulation using a differential equation.

1.2.6 Field-Effect Transistors: Large-Signal Modeling

While the integration of small-signal FET models into the FDTD simulation provides an important simulation tool for active microwave circuits, modern applications of the FET routinely use nonlinear regions of operation. Amplifiers operating outside of class A conditions are significantly more energy efficient but are more complex to design and optimize. Indeed, an accurate full-wave simulation is an important tool in the design of nonlinear amplifiers.

The nonlinear properties of a transistor may be incorporated into a circuit model using a combination of approaches. First, controlled current sources, such as I_d in Figure 1.5, may be controlled by nonlinear or transcendental functions of voltage or current elsewhere in the circuit: this approach was used to model the junction diode in Section 1.2.1. Second, values of circuit elements such as resistors and capacitors may depend upon voltages or currents in the circuit, possibly by a nonlinear function. Finally, nonlinear effects may be emulated by the introduction of junction diodes into the circuit model.

In one approach [26], the metal semiconductor field effect transistor (MESFET) model similar to that of Curtice [27] was used to simulate a nonlinear amplifier

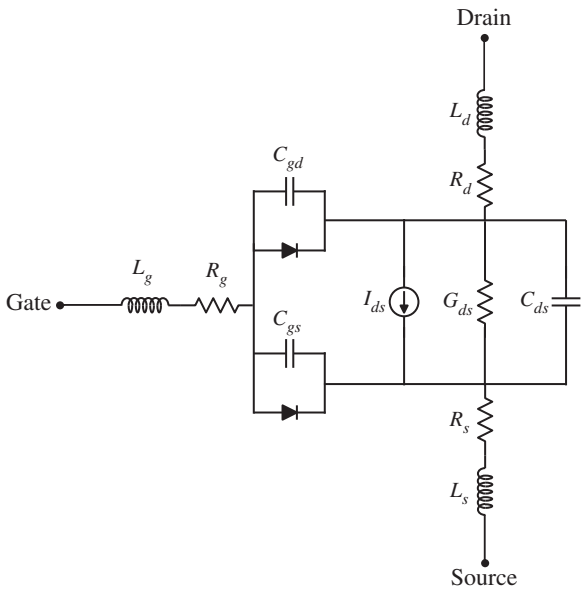

Figure 1.6 Nonlinear FET model.

circuit. The transistor model used is illustrated in schematic form in Figure 1.6: the nonlinear current source I_{ds} is represented in terms of the voltages at the source, gate, and drain terminals as follows:

$$I_{ds} = \begin{cases} \beta(1 + \lambda V_{ds})(V_{gs} - V_{to})^2 \tanh(\alpha V_{ds}) & \text{if } V_{gs} > V_{to} \\ 0 & \text{if } V_{gs} < V_{to} \end{cases} \tag{1.28}$$

where the parameters α, β, and λ are specific to the construction of the transistor, and V_{to} is the threshold voltage of the transistor.

In the approach of [26], the lumped components L_d, R_d, L_g, R_g, L_s, and R_s were each placed into their own FDTD cell and simulated using the approach of [6]. Similarly, each pairing of diode and parallel capacitance occupied its own cell, and these were simulated according to the approach of [12]. Finally, the parallel combination of $I_{ds} \| R_{ds} \| C_{ds}$ was addressed using a nonlinear FDTD updating formulation, which was solved numerically at each time step using Newton–Raphson iteration [28].

A similar work was performed by Kuo et al., wherein the model of Figure 1.5 was extended through a nonlinear capacitance C_{gs} and a nonlinear source for I_{ds}. The nonlinear capacitance is controlled by the following formula:

$$C_{gs}(v_g) = \frac{C_{gs0}}{\sqrt{1 - \frac{v_g}{\phi_{bi}}}} \tag{1.29}$$

and the drain current is a function of both external and internal node voltages:

$$I_{ds}\left(v_d, v_{G'S'}\right) = \left(A_0 + A_1 v_{G'S'} + A_2 v_{G'S'}^2 + A_3 v_{G'S'}^3\right) \tanh(\alpha v_d) \tag{1.30}$$

Table 1.2 Description of numerical constants for the MESFET model.

Symbol	Description	Value	Unit
R_g, R_d	Gate, drain resistance	0.5	Ω
R_s	Source resistance	0.7	Ω
R_i	Intrinsic resistance	1.0	Ω
L_g, L_d	Gate, drain inductance	0.05	nH
L_S	Source inductance	0.1	nH
C_{gd}	Gate–drain capacitance	0.2	pF
C_{ds}	Drain–source capacitance	0.6	pF
C_{gs0}	Zero-bias gate capacitance	3	pF
A_0	Model coefficients	0.5304	
A_1		0.2595	
A_2		–0.0542	
A_3		–0.0305	
α	Hyperbolic tangent parameter	1.0	

The numerical constants used for the MESFET in [29] are listed in Table 1.2.

Unlike the approaches of [24, 25], where only the linear operation of the MESFET was addressed, and also unlike the approach of [26], where lumped components were modeled separately within the FDTD simulation, the simulation approach of [29] encapsulates the entire transistor model into a single FDTD cell. The five nonlinear state equations of the MESFET model, including the internal node voltages G', S', and D', as well as the total voltage across the FDTD cell are converted into a matrix form, and solved iteratively at each time step using the Newton–Raphson approach. Nonlinear behavior of the device was shown in the form of compression in the amplifier's output power and in the appearance of 2nd and 3rd harmonic components, as the input signal power was increased.

Simulation of active devices within FDTD poses an additional challenge in the form of coupling between device leads. In an active device with a high gain, there is a strong possibility for coupling between the device leads leading to unwanted self-oscillation of the circuit. In a work similar to [29], Chen and Fusco placed a section of simulated absorbing boundary between the gate and drain terminals of an FET [30].

The approach of [29] was further extended by modifying the interface region between the simulated active device and the conducting transmission line [31]. By modeling the device as a pair of "active sheets," with the capability for varying the cross-sectional voltage, it is possible to effectively match the simulated nonlinear device to modes on the transmission line. Mode matching and launching is an important area of consideration for the FDTD simulation of planar circuits and in

particular for the simulation of circuit elements. This topic is further discussed in [32–34].

Many FDTD simulation packages incorporate simulation elements such as voltage probes, current probes, and voltage sources as preprogrammed software modules. Where possible, it is advantageous to reuse such modules instead of writing and testing specialized updating equations for each new type of component. Mix et al. used a modified Curtice MESFET model, where incoming currents are determined by magnetic field integration around the conducting terminals of the MESFET device [35]. In turn, the MESFET's response was emulated in the FDTD simulation by means of a controlled voltage source. In this simplified model, an explicit formulation was used for the Curtice MESFET equations, so that an iterative solution was not required. This approach reduces the computational complexity of the simulation, but at the possible cost of accuracy and stability.

1.3 FDTD–SPICE

In many of the examples discussed earlier in the chapter, simulation of a new type of circuit element required the development of an entirely new FDTD updating formulation, specialized to that device type. It is advantageous to connect an FDTD simulation to an external solver, which is already equipped with a variety of device models. The well-known SPICE circuit simulator is one such software, and is considered the industry standard for analog circuit simulation. In this program, arbitrary arrangements of passive, active, and nonlinear components can be constructed and simulated in the time or frequency domain [36].

A simulator combining the capabilities of FDTD and SPICE was demonstrated by Piket-May [5, 6]. In this approach, Ampere's law is written as follows:

$$\varepsilon \frac{\partial \vec{E}}{\partial t} + \vec{J}(\vec{E}) = \nabla \times \vec{H} \tag{1.31}$$

where $\vec{J}(\vec{E})$ represents the current through a circuit component as a function of the electric field across it. In terms of an electrical circuit (1.31) may be rewritten as follows:

$$C\frac{dV}{dt} + I_{\text{SPICE}}(V) = I_{\text{total}} \tag{1.32}$$

where I_{total} is the total current through the FDTD cell and C is the capacitance of the cell. For a Z-directed lumped element, C can be found as follows:

$$C = \frac{\varepsilon \Delta x \Delta y}{\Delta z} \tag{1.33}$$

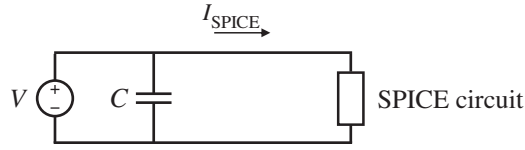

Figure 1.7 Schematic illustration of FDTD–SPICE integration.

From the perspective of the SPICE simulator, a circuit similar to that in Figure 1.7 is constructed. In this illustration, a one-port (two-terminal) device is illustrated, though the technique is extensible to networks of many ports. At each time step, voltage V is updated based on the electric field within the FDTD cell. Current I is a function of voltage V and the response of the circuit to be modeled (labeled "SPICE Circuit").

At each simulation time step, the FDTD–SPICE interaction occurs one time. Voltage V is updated in the SPICE simulation, and then current I_{SPICE} is retrieved and updated in the FDTD simulation by means of current density J. One disadvantage to this approach occurs because FDTD and SPICE address the updating of voltage and current in different ways. In SPICE, both voltages and currents are updated simultaneously at each time step. Conversely, in FDTD, the electric and magnetic fields are updated in a "leapfrog" manner.

In the ideal case, the value of voltage V supplied to the SPICE simulation will be based on an average of $E_z|_{i,j,k}^{n}$ and $E_z|_{i,j,k}^{n+1}$, because current I_{SPICE} must be valid at time $n+\frac{1}{2}$. Inserting (1.32) into (1.1) leads to an electric-field updating formulation of:

$$\begin{aligned} E_z|_{i,j,k}^{n+1} = {} & \frac{2\varepsilon_z|_{i,j,k} - \Delta t\,\sigma_z^e|_{i,j,k}}{2\varepsilon_z|_{i,j,k} + \Delta t\,\sigma_z^e|_{i,j,k}} E_z|_{i,j,k}^{n} \\ & + \frac{2\Delta t}{\left(2\varepsilon_z|_{i,j,k} + \Delta t\,\sigma_z^e|_{i,j,k}\right)\Delta x}\left(H_y\big|_{i,j,k}^{n+\frac{1}{2}} - H_y\big|_{i-1,j,k}^{n+\frac{1}{2}}\right) \\ & - \frac{2\Delta t}{\left(2\varepsilon_z|_{i,j,k} + \Delta t\,\sigma_z^e|_{i,j,k}\right)\Delta y}\left(H_x\big|_{i,j,k}^{n+\frac{1}{2}} - H_x\big|_{i,j-1,k}^{n+\frac{1}{2}}\right) \\ & - \frac{2\Delta t}{2\varepsilon_z|_{i,j,k} + \Delta t\,\sigma_z^e|_{i,j,k}} \frac{I_{\text{SPICE}}\left(\dfrac{\Delta z\left(E_z|_{i,j,k}^{n} + E_z|_{i,j,k}^{n+1}\right)}{2}\right)}{\Delta x \Delta y} \end{aligned} \tag{1.34}$$

While this equation is numerically implicit, it is not possible to solve using a traditional SPICE simulator, because the value of $E_z|_{i,j,k}^{n+1}$ is not known at the time when the SPICE function is executed. Thus, an explicit form is required:

$$\begin{aligned} E_z|_{i,j,k}^{n+1} = {} & \frac{2\varepsilon_z|_{i,j,k} - \Delta t\,\sigma_z^e|_{i,j,k}}{2\varepsilon_z|_{i,j,k} + \Delta t\,\sigma_z^e|_{i,j,k}} E_z|_{i,j,k}^{n} \\ & + \frac{2\Delta t}{\left(2\varepsilon_z|_{i,j,k} + \Delta t\,\sigma_z^e|_{i,j,k}\right)\Delta x}\left(H_y|_{i,j,k}^{n+\frac{1}{2}} - H_y|_{i-1,j,k}^{n+\frac{1}{2}}\right) \\ & - \frac{2\Delta t}{\left(2\varepsilon_z|_{i,j,k} + \Delta t\,\sigma_z^e|_{i,j,k}\right)\Delta y}\left(H_x|_{i,j,k}^{n+\frac{1}{2}} - H_x|_{i,j-1,k}^{n+\frac{1}{2}}\right) \\ & - \frac{2\Delta t}{2\varepsilon_z|_{i,j,k} + \Delta t\,\sigma_z^e|_{i,j,k}} \frac{I_{\text{SPICE}}\left(E_z|_{i,j,k}^{n}\right)}{\Delta x \Delta y} \end{aligned} \tag{1.35}$$

This explicit formulation is practical to solve on an unmodified SPICE software, but using an explicit formulation may lead to accuracy or stability problems. Indeed, Piket-May noted that certain configurations of an FDTD–SPICE amplifier simulation had diverging solutions [5]. Similarly, Thomas et al. noted that an FDTD–SPICE simulation of a digital circuit suffered from low accuracy at high frequencies [22]. Also, it was noted that certain circuits may be impossible to simulate using this configuration and the use of the poisson and continuity equation solver (PISCES) simulator [37] was suggested in place of SPICE [38].

The explicit nature of the FDTD–SPICE updating formulation was observed by Li and Sui, who proposed an alternative technique based on solving for I_{SPICE} at time step $n+1$ instead of $n+\frac{1}{2}$ [39]. In this approach, the SPICE simulation is supplied with a current value from the FDTD simulation, taken at time $n+\frac{1}{2}$. Within the SPICE netlist, this current is represented as a Norton-equivalent current source with a parallel resistance R_{grid}. The resulting current into the SPICE-simulated circuit is updated back into the FDTD simulation at time $n+1$. This method allowed to simulate both passive and active circuits, including a mixer and pulse generator, demonstrating accuracy at even high frequencies and nonlinear operating conditions [39, 40].

In many cases, time steps employed in SPICE simulators are varied depending on the convergence of nonlinear updating equations. In situations that render this convergence difficult, such as rapid changes in voltage or highly nonlinear device operation, the time step is reduced [41]. Sui noted that an FDTD–SPICE simulator can operate with variable Δt. During normal operation, the time step is chosen according to the CFL condition – the maximum possible for an FDTD simulation. When poor convergence is detected within the SPICE simulator, the time step may be reduced in both FDTD and SPICE to account for this. Such a method allows for improved accuracy and stability while maintaining computational efficiency [42].

1.4 Data-Based Models

In the previously described approaches for the incorporation of lumped-element circuits into FDTD simulations, the circuit components were described in the form of physical models. Such models may be represented by a single schematic symbol, as in the case of the junction diode, or they may be represented by complex sub-circuits, such as the MESFET model illustrated in Figure 1.6. In all cases, the physics of the sub-circuits are modeled by the values of circuit components and by the mathematical formulas used to update dependent voltage sources and nonlinear circuit components.

In many cases, it may be impractical or fully impossible to acquire an exact physical model of a circuit component. If the physical details of a component (material composition, geometry) are available, then a physical model may be generated by numerical simulations of the semiconductor's operation. If the device can be acquired and measured in the laboratory, then the device parameters may be extracted [23]. However, exact internal details of a device may be unavailable due to intellectual property restrictions, and transistor parameter extraction in the laboratory requires specialized equipment and skills.

It is desirable to be able to simulate a device based on characteristics that have been measured in the laboratory or provided by the manufacturer. For linear devices, the common language of device description is *S*-parameters: they may be measured in most microwave laboratories using a vector network analyzer. Also, many component manufacturers provide *S*-parameter data for the devices they sell. For nonlinear components, an emerging characterization is *X*-parameters, which describe a component in terms of its harmonic response to an input signal [43].

1.4.1 Linear Lumped Elements: *S*-Parameter Approaches

While FDTD is a time-domain technique, it lends itself well to extraction of *S*-parameters from simulation results through a Fourier transform of electric and magnetic field results. The reverse case has also been demonstrated: inserting lumped elements into FDTD simulations, which are described by their *S*-parameters. This is a useful approach for characterizing a device whose parameters have already been measured in the context of a larger microwave device such as an antenna or transmission line. Because the *S*-parameters only address the linear operation of circuit components, only a superficial review will be presented for this topic.

In the approach of Zhang and Wang [44], thse scattering **S** matrix is converted into an admittance **Y** matrix, using a method such as that described by Pozar [20]. For a two-port network, the current at each port can be calculated in the

frequency domain as the matrix product of the admittance matrix and the port voltages:

$$\begin{bmatrix} I_1(\omega) \\ I_2(\omega) \end{bmatrix} = \begin{bmatrix} Y_{11}(\omega) & Y_{12}(\omega) \\ Y_{22}(\omega) & Y_{22}(\omega) \end{bmatrix} \begin{bmatrix} V_1(\omega) \\ V_2(\omega) \end{bmatrix} \tag{1.36}$$

For a time-domain simulation, voltages must be updated at discrete time steps. The inverse Fourier transforms of the admittance terms are taken to provide time-domain admittance parameters:

$$\widehat{Y}_{i,j}(t) = \mathcal{F}^{-1}(Y_{i,j}(\omega)) \tag{1.37}$$

At each time step, the currents at two ports of the network can be found by convolving the time-domain admittance with the port voltages:

$$\begin{aligned} I_1(t) &= \widehat{Y}_{11}(t) * V_1(t) + \widehat{Y}_{12}(t) * V_2(t) \\ I_2(t) &= \widehat{Y}_{21}(t) * V_1(t) + \widehat{Y}_{22}(t) * V_2(t) \end{aligned} \tag{1.38}$$

For example, the current in the z direction at port 1 of the network, as a function of all previous voltages, can be written as [44]:

$$I_z\big|_{\text{port 1}}^{n+\frac{1}{2}} = \Delta z \sum_{k=1}^{n} \left[\widehat{Y}_{11}(k)\, E_z\big|_{\text{port 1}}^{n-k} + \widehat{Y}_{12}(k)\, E_z\big|_{\text{port 2}}^{n-k} \right] \tag{1.39}$$

We note that while the required convolution is performed in this formulation, it is an explicit formulation because the value of $E_z|^{n+1}$ is not considered, which may limit accuracy at large time steps. An extension of this technique was described by Ye and Drewniak, wherein the generalized pencil-of-function technique was used to convert the time-domain Y-parameters into a series of exponential functions [45]. This approach reduces memory consumption and computational time for the simulation.

Pereda et al. described an extension to the embedding of arbitrary lumped elements into the FDTD grid [46]. In their approach, the impedance of the network is transformed to the Laplace domain and approximated by means of a bilinear transformation. This bilinear expression forms the basis for a set of updating equations that have implicit formulation and, therefore, match the central difference scheme of the FDTD method.

Numerous additional schemes have been described for the incorporation of arbitrary linear lumped elements into FDTD simulations. For example, the work of Pereda et al. was extended by Gonzalez and Pereda to two-port [47] and active [48] networks, using a similar bilinear approach to [46]. Other techniques have been developed to reduce computational load, such as the use of recursive techniques [49, 50]. Also, methods are available for the incorporation of linear lumped elements based on their circuit models, such as [51–54].

1.4.2 Nonlinear Lumped Elements: *X*-Parameters

As noted in the previous section, *S*-parameters can be used to model active devices such as amplifiers. However, the use of *S*-parameters for active-device modeling is limited to linear cases. Two factors limit the applicability of *S*-parameters in the modeling of nonlinear devices. First, *S*-parameters are considered on a frequency-by-frequency basis. A signal at frequency ω_1 will not affect a device's response to a signal being transmitted simultaneously at frequency ω_2. Second, *S*-parameters do not consider the capability for a device to generate harmonics: for example, when a signal at frequency ω_1 enters a nonlinear device, we may see signals of $2\omega_1$, $3\omega_1$, etc. propagating from the device's ports. To properly address these effects, an alternative model is needed.

One such solution is offered by *X*-parameters [55]. In this approach, nonlinear responses of a device are linearized in the frequency domain around a specific operating frequency. For example, an amplifier can be excited with a frequency ω_1 at port 1. Then, small additional signals of frequencies $[\omega_1, 2\omega_1 \ldots, K\omega_1]$ are applied to the network, and changes in the outgoing waves are measured, again at the frequencies $[\omega_1, 2\omega_1 \ldots, K\omega_1]$.

In the nomenclature of *X*-parameters, waves incident on a network are written as $A_{q,l}$, where q is the index of the port and l is the index of the harmonic ($l = 1$ is the fundamental frequency of the excitation signal). Waves propagating outward from the network are written as $B_{p,k}$, again with p referring to the port index and k the harmonic. The outgoing wave $B_{p,k}$ can be approximated as [43]:

$$B_{p,k} \cong X_{p,k}^{(FB)} P^k + \sum_{\substack{q=1 \\ (q,l)\neq(1,1)}}^{\substack{q=N \\ l=K \\ l=1}} \left[X_{p,k;q,l}^{(S)} A_{q,l} P^{k-l} + X_{p,k;q,l}^{(T)} A_{q,l}^{*} P^{k+l} \right] \tag{1.40}$$

In place of the $N \times N$ matrix of the *S*-parameters, there are three matrices of *X*-parameters required for this formulation. The parameter $X_{p,k}^{(FB)}$ is a matrix of dimension $N \times K$ (for a system with N ports and where K harmonics are considered) describing the device's large-signal response. The parameters $X_{p,k;q,l}^{(S)}$ and $X_{p,k;q,l}^{(T)}$ both have dimension $N \times K \times N \times K$, and describe the small changes in the outgoing waves $B_{p,k}$, based on small changes in the incoming signals $A_{q,l}$ at any port and harmonic. The constant P serves the purpose of phase normalization and has the value $P = e^{j\angle A_{1,1}}$.

Kast and Elsherbeni described the extraction of large-signal $\left(X_{p,k}^{(FB)}\right)$ *X*-parameters from the simulation of a one-port circuit containing a junction diode [55]. In this approach, a discrete Fourier transform was used to convert

voltages and currents at the network ports into the frequency domain for each of the harmonics. This approach was extended to a two-port case, where both large-signal and small-signal $\left(X^{(S)}_{p,k;q,l}, X^{(T)}_{p,k;q,l}\right)$ terms were extracted from the simulation results [56]. While these techniques do not yet provide a method for simulating a device based on its X-parameters, they create a necessary foundation for the further study of nonlinear devices within FDTD simulations.

1.5 Conclusions

Myriad applications of RF and microwave technologies depend on nonlinear components to achieve their desired function. Indeed, at a fundamental level, all real-world RF active devices and amplifiers are nonlinear components, and RF oscillators require the presence of a nonlinear component to operate [57]. In this context, we find that the capability to simulate nonlinear circuit components is a valuable asset to any microwave simulation technique. Indeed, the FDTD technique is extremely well suited to simulation of nonlinear devices due to its time-domain nature: nonlinear components may be directly embedded into the FDTD updating formulation, and results extracted in the time domain, or converted into the frequency domain allowing evaluation of harmonics and other effects.

References

1 Sui, W. (1991). *An Extended Finite Difference Time Domain Method for Hybrid Electromagnetic Systems with Active and Passive Lumped Elements*. University of Utah.

2 W. Sui, D. A. Christensen, and C. H. Durney, "Extending the two-dimensional FDTD method to hybrid electromagnetic systems with active and passive lumped elements," *IEEE Transactions on Microwave Theory and Techniques*, vol. 40, no. 4, pp. 724–730, Apr. 1992, doi: https://doi.org/10.1109/22.127522.

3 P. B. Johns, "On the relationship between TLM and finite-difference methods for Maxwell's equations (short paper)," *IEEE Transactions on Microwave Theory and Techniques*, vol. 35, no. 1, pp. 60–61, Jan. 1987, doi: https://doi.org/10.1109/TMTT.1987.1133595.

4 R. H. Voelker and R. J. Lomax, "A finite-difference transmission line matrix method incorporating a nonlinear device model," *IEEE Transactions on Microwave Theory and Techniques*, vol. 38, no. 3, pp. 302–312, Mar. 1990, doi: https://doi.org/10.1109/22.45349.

5 Piket-May, M.J. (2021). Three-dimensional time-domain numerical studies of pulse behavior in digital interconnect circuits with passive and active loads. PhD Northwestern University, United States – Illinois. https://www.proquest.com/docview/304057910/abstract/B04340F3C8194D1APQ/1 (accessed 20 June 2022).

6 Piket-May, M., Taflove, A., and Baron, J. (1994). FD-TD modeling of digital signal propagation in 3-D circuits with passive and active loads. *IEEE Transactions on Microwave Theory and Techniques* 42 (8): 1514–1523. https://doi.org/10.1109/22.297814.

7 J. J. Ebers and J. L. Moll, "Large-signal behavior of junction transistors," *Proceedings of the IRE*, vol. 42, no. 12, pp. 1761–1772, Dec. 1954, doi: https://doi.org/10.1109/JRPROC.1954.274797.

8 Nagel, L.W. (1970). SPICE2: a computer program to simulate semiconductor circuits. PhD Dissertations University of California, Berkeley. https://ci.nii.ac.jp/naid/10014667404/ (accessed 30 June 2022).

9 Massobrio, G. and Antognetti, P. (1998). *Semiconductor Device Modeling*, 1e. New York: McGraw-Hill Education.

10 Elsherbeni, A.Z. and Demir, V. (2016). *The finite-difference time-domain method for electromagnetics with MATLAB simulations*, ACES Series on Computational Electromagnetics and Engineering, 2e. Edison, NJ: SciTech Publishing, an Imprint of IET.

11 W. Shockley, "The theory of p-n junctions in semiconductors and p–n junction transistors," *Bell System Technical Journal*, vol. 28, no. 3, pp. 435–489, Jul. 1949, doi: https://doi.org/10.1002/j.1538-7305.1949.tb03645.x.

12 P. Ciampolini, P. Mezzanotte, L. Roselli, D. Sereni, R. Sorrentino, and P. Torti, "Simulation of HF circuits with FDTD technique including non-ideal lumped elements," in *Proceedings of 1995 IEEE MTT-S International Microwave Symposium*, May 1995, pp. 361–364 vol. 2. doi: https://doi.org/10.1109/MWSYM.1995.405969.

13 Sedra, A.S. and Smith, K.C. (2014). *Microelectronic Circuits*, The Oxford Series in Electrical and Computer Engineering, 7e. New York, NY: Oxford University Press.

14 ElMahgoub, K. and Elsherbeni, A.Z. (2014). FDTD implementations of integrated dependent sources in full-wave electromagnetic simulations. *Applied Computational Electromagnetics Society (ACES) Journal* 29 (12): 10.

15 P. Ciampolini, P. Mezzanotte, L. Roselli, and R. Sorrentino, "Accurate and efficient circuit simulation with lumped-element FDTD technique," *IEEE Transactions on Microwave Theory and Techniques*, vol. 44, no. 12, pp. 2207–2215, Dec. 1996, doi: https://doi.org/10.1109/22.556448.

16 H. K. Gummel and H. C. Poon, "An integral charge control model of bipolar transistors," *Bell System Technical Journal*, vol. 49, no. 5, pp. 827–852, May 1970, doi: https://doi.org/10.1002/j.1538-7305.1970.tb01803.x.

17 F. Kung and H. T. Chuah, "Modeling of bipolar junction transistor in FDTD simulation of printed circuit board," *Progress In Electromagnetics Research*, vol. 36, pp. 179–192, 2002, doi: https://doi.org/10.2528/PIER02013001.

18 Bahl, I. (2009). *Fundamentals of RF and Microwave Transistor Amplifiers*, 1e. Hoboken, N.J: Wiley-Interscience.

19 Razavi, B. (2011). *RF Microelectronics*, 2e. Upper Saddle River, NJ: Prentice Hall.

20 Pozar, D.M. (2011). *Microwave Engineering*, 4e. Hoboken, NJ: Wiley.

21 Ludwig, R. and Bogdanov, G. (2008). *RF Circuit Design: Theory & Applications*, 2e. Upper Saddle River, NJ: Pearson.

22 V. A. Thomas, M. E. Jones, M. Piket-May, A. Taflove, and E. Harrigan, "The use of SPICE lumped circuits as sub-grid models for FDTD analysis," *IEEE Microwave and Guided Wave Letters*, vol. 4, no. 5, pp. 141–143, May 1994, doi: https://doi.org/10.1109/75.289516.

23 Kompa, G. (2019). *Parameter Extraction and Complex Nonlinear Transistor Models*. Artech House.

24 Chien-Nan Kuo, B.H, and T. Itoh, "FDTD analysis of active circuits with equivalent current source approach," in *IEEE Antennas and Propagation Society International Symposium. 1995 Digest*, Jun. 1995, vol. 3, pp. 1510–1513. doi: https://doi.org/10.1109/APS.1995.530863.

25 Chien-Nan Kuo, V. A. Thomas, Siou Teck Chew, B. Houshmand, and T. Itoh, "Small signal analysis of active circuits using FDTD algorithm," *IEEE Microwave and Guided Wave Letters*, vol. 5, no. 7, pp. 216–218, 1995, doi: https://doi.org/10.1109/75.392279.

26 M. Matteucci, P. Mezzanotte, L. Roselli, and P. Ciampolini, "Numerical analysis of electronic circuits with FDTD-LE technique," *WIT Transactions on Engineering Sciences*, vol. 11, 1996, doi: https://doi.org/10.2495/ES960211.

27 W. R. Curtice, "A MESFET model for use in the design of GaAs integrated circuits," *IEEE Transactions on Microwave Theory and Techniques*, vol. 28, no. 5, pp. 448–456, May 1980, doi: https://doi.org/10.1109/TMTT.1980.1130099.

28 P. Ciampolini, P. Mezzanotte, L. Roselli, and R. Sorrentino, "Efficient simulation of high speed digital circuits using time adaptive FD-TD technique," in *1995 25th European Microwave Conference*, IEEE, 1995, vol. 2, pp. 636–640. doi: https://doi.org/10.1109/EUMA.1995.337038.

29 Chien-Nan Kuo, B. Houshmand, and T. Itoh, "Full-wave analysis of packaged microwave circuits with active and nonlinear devices: an FDTD approach," *IEEE Transactions on Microwave Theory and Techniques*, vol. 45, no. 5, pp. 819–826, 1997, doi: https://doi.org/10.1109/22.575606.

30 Q. Chen and V. F. Fusco, "Hybrid FDTD large-signal modeling of three-terminal active devices," *IEEE Transactions on Microwave Theory and Techniques*, vol. 45, no. 8, pp. 1267–1270, Aug. 1997, doi: https://doi.org/10.1109/22.618419.

31 V. S. Reddy and R. Garg, "An improved extended FDTD formulation for active microwave circuits," *IEEE Transactions on Microwave Theory and Techniques*, vol. 47, no. 9, pp. 1603–1608, Sep. 1999, doi: https://doi.org/10.1109/22.788599.

32 I. Wolff, "Finite difference time-domain simulation of electromagnetic fields and microwave circuits," *International Journal of Numerical Modelling: Electronic Networks, Devices and Fields*, vol. 5, no. 3, pp. 163–182, 1992, doi: https://doi.org/10.1002/jnm.1660050306.

33 C. H. Durney, Wenquan Sui, D. A. Christensen, and Jingyi Zhu, "A general formulation for connecting sources and passive lumped-circuit elements across multiple 3-D FDTD cells," *Microwave and Guided Wave Letters*, vol. 6, no. 2, pp. 85-, 1996, doi: https://doi.org/10.1109/75.481997.

34 W. K. Gwarek and M. Celuch-Marcysiak, "Wide-band *S*-parameter extraction from FD-TD simulations for propagating and evanescent modes in inhomogeneous guides," *IEEE Transactions on Microwave Theory and Techniques*, vol. 51, no. 8, pp. 1920–1928, Aug. 2003, doi: https://doi.org/10.1109/TMTT.2003.815265.

35 Mix, J., Dixon, J., Popovic, Z., and Piket-May, M. (1999). Incorporating non-linear lumped elements in FDTD: the equivalent source method. *International Journal of Numerical Modelling: Electronic Networks, Devices and Fields* 12 (1–2): 157–170.

36 Vladimirescu, A. (1994). *The SPICE Book*. New York: John Wiley & Sons.

37 Pinto, M.R., Rafferty, C.S., and Dutton, R.W. (1984). *PISCES II: Poisson and Continuity Solver*. Stanford, CA: Stanford Electronics Laboratories, Stanford University.

38 V. A. Thomas, M. E. Jones, and R. J. Mason, "Coupling of the PISCES device modeler to a 3-D Maxwell FDTD solver," *IEEE Transactions on Microwave Theory and Techniques*, vol. 43, no. 9, pp. 2170–2172, Sep. 1995, doi: https://doi.org/10.1109/22.414557.

39 Li, T. (1999). *FDTD-Based Full Wave Co-simulation Model for Hybrid Electromagnetic Systems*. Newark, NJ: New Jersey Institute of Technology.

40 T. Li and W. Sui, "Extending Spice-like analog simulator with a time-domain full-wave field solver," in *2001 IEEE MTT-S International Microwave Symposium Digest (Cat. No.01CH37157)*, 2001, vol. 2, pp. 1023–1026doi: https://doi.org/10.1109/MWSYM.2001.967066.

41 Najm, F.N. (2010). *Circuit Simulation*. Hoboken, NJ: John Wiley & Sons.

42 Sui, W. (2001). *Time-Domain Computer Analysis of Nonlinear Hybrid Systems*. CRC Press.

43 Root, D., Verspecht, J., Horn, J., and Marcu, M. (2013). *X-Parameters: Characterization, Modeling, and Design of Nonlinear RF and Microwave Components*. Cambridge University Press.

44 Jiazong Zhang and Yunyi Wang, "FDTD analysis of active circuits based on the *S*-parameters [microwave hybrid ICs]," in *Proceedings of 1997 Asia-Pacific Microwave Conference*, IEEE, Dec. 1997, vol. 3, pp. 1049–1052. doi: https://doi.org/10.1109/APMC.1997.656395.

45 X. Ye and J. L. Drewniak, "Incorporating two-port networks with S-parameters into FDTD," *IEEE Microwave and Wireless Components Letters*, vol. 11, no. 2, pp. 77–79, Feb. 2001, doi: https://doi.org/10.1109/7260.914308.

46 J. A. Pereda, F. Alimenti, P. Mezzanotte, L. Roselli, and R. Sorrentino, "A new algorithm for the incorporation of arbitrary linear lumped networks into FDTD simulators," *IEEE Transactions on Microwave Theory and Techniques*, vol. 47, no. 6, pp. 943–949, Jun. 1999, doi: https://doi.org/10.1109/22.769330.

47 O. Gonzalez, J. A. Pereda, A. Herrera, and A. Vegas, "An extension of the lumped-network FDTD method to linear two-port lumped circuits," *IEEE Transactions on Microwave Theory and Techniques*, vol. 54, no. 7, pp. 3045–3051, Jul. 2006, doi: https://doi.org/10.1109/TMTT.2006.877058.

48 O. Gonzalez, J. A. Pereda, A. Herrera, A. Grande, and A. Vegas, "Combining the FDTD method and rational-fitting techniques for modeling active devices characterized by measured S -parameters," *IEEE Microwave and Wireless Components Letters*, vol. 17, no. 7, pp. 477–479, 2007, doi: https://doi.org/10.1109/LMWC.2007.899292.

49 Jung-Yub Lee, Jeong-Hae Lee, and Hyun-Kyo Jung, "Linear lumped loads in the FDTD method using piecewise linear recursive convolution method," *IEEE Microwave and Wireless Components Letters*, vol. 16, no. 4, pp. 158–160, Apr. 2006, doi: https://doi.org/10.1109/LMWC.2006.872148.

50 C. Wang and C. Kuo, "An efficient scheme for processing arbitrary lumped multiport devices in the finite-difference time-domain method," *IEEE Transactions on Microwave Theory and Techniques*, vol. 55, no. 5, pp. 958–965, May 2007, doi: https://doi.org/10.1109/TMTT.2007.895652.

51 H. E. A. El-Raouf, W. Yu, and R. Mittra, "Application of the Z-transform technique to modelling linear lumped loads in the FDTD," *IEE Proceedings - Microwaves, Antennas and Propagation*, vol. 151, no. 1, pp. 67–70, Feb. 2004, doi: https://doi.org/10.1049/ip-map:20040067.

52 Tzong-Lin Wu, Sin-Ting Chen, and Yi-Shang Huang, "A novel approach for the incorporation of arbitrary linear lumped network into FDTD method," *IEEE Microwave and Wireless Components Letters*, vol. 14, no. 2, pp. 74–76, Feb. 2004, doi: https://doi.org/10.1109/LMWC.2003.822567.

53 Zhenhai Shao and M. Fujise, "An improved FDTD formulation for general linear lumped microwave circuits based on matrix theory," *IEEE Transactions*

on Microwave Theory and Techniques, vol. 53, no. 7, pp. 2261–2266, 2005, doi: https://doi.org/10.1109/TMTT.2005.850450.

54 Demir, V. (2016). Formulations for modeling voltage sources with RLC impedances in the FDTD method. *The Applied Computational Electromagnetics Society Journal (ACES)* 31 (9): 1020–1027.

55 J. M. Kast and A. Z. Elsherbeni, "Extraction of nonlinear X-parameters from FDTD simulation of a one-port device," in *2021 United States National Committee of URSI National Radio Science Meeting (USNC-URSI NRSM)*, Jan. 2021, pp. 89–90. doi: https://doi.org/10.23919/USNC-URSINRSM51531.2021.9336444.

56 J. M. Kast and A. Z. Elsherbeni, "Extraction of X-parameters from FDTD simulation of a two-port nonlinear circuit," *2021 International Applied Computational Electromagnetics Society Symposium (ACES)*, , Aug. 2021.

57 Pedro, J.C., Root, D.E., Xu, J., and Nunes, L.C. (2018). *Nonlinear Circuit Simulation and Modeling: Fundamentals for Microwave Design*, 1e, 1–44. Cambridge, Cambridge University Press.